Electron-impact excitation of the $3s3p\ ^1P^o$ state of Mg-like ions: S^{4+}, Ar^{6+}, and Ca^{8+}

Takeshi Kai,[1] Rajesh Srivastava,[2] and Shinobu Nakazaki[1,*]
[1]*Department of Applied Physics, Faculty of Engineering, University of Miyazaki, Miyazaki 889-2192, Japan*
[2]*Department of Physics, Indian Institute of Technology, Roorkee-247667, India*
(Received 23 June 2004; published 6 December 2004; publisher error corrected 17 December 2004)

Electron-impact excitation of the $3s3p\ ^1P^o$ state of Mg-like ions (S^{4+}, Ar^{6+}, and Ca^{8+}) from their ground state is studied theoretically using the *R*-matrix method with 31 target states. Results are reported in the range of low incident electron energies for the total and differential cross sections of this excitation process as well as for the polarization fraction and the Stokes parameters P_1, P_2, and P_3 of the photons emitted on the decay of the excited $3s3p\ ^1P^o$ state to the ground state. The agreement between experiment and the present results is good. We obtain a polarization fraction of about 35% at low incident electron energies in these ions.

DOI: 10.1103/PhysRevA.70.062705 PACS number(s): 34.80.Kw

I. INTRODUCTION

Electron-impact excitation processes in ions are of special importance in hot plasmas such as solar corona and fusion plasmas. Their studies are also now a subject of laboratory experiment [1]. In recent years, due to developments in the experimental technology, measurements have been made [2–8] of the total cross section (TCS) and differential cross section (DCS) for Mg-like ions, which are of interest to theorists for comparison with theoretical calculations.

For electron-impact excitation in the S^{4+}, Ar^{6+}, and Ca^{8+} ions, various theoretical and experimental TCS results have been reported. Dufton and Kingston [9] have presented collision strengths of S^{4+} for the $3s3p\ ^{1,3}P^o$ excitation using the *R*-matrix method with eight target states. In 1993, Griffin *et al.* [10] calculated the TCS of Ar^{6+} for the three transitions $3s^2\ ^1S^e \rightarrow 3s3p\ ^{1,3}P^o$ and $3s3p\ ^3P^o \rightarrow 3s3p\ ^1P^o$ using the *R*-matrix method with eight target states. The TCS for the $3s3p\ ^{1,3}P^o$ excitation in Ar^{6+} has been measured by Chung *et al.* [3]. Wallbank *et al.* [8] have measured the TCS of S^{4+} for the $3s3p\ ^{1,3}P^o$ excitation.

For the DCS, there are only a few previous reports. Griffin *et al.* [10] calculated the DCS of Ar^{6+} for the $3s^2\ ^1S^e \rightarrow 3s3p\ ^1P^o$ transition using the *R*-matrix method with a simple two-state calculation at energies 1.05 and 2.00 times the threshold excitation energy. Jalabert *et al.* [2] measured the DCS of Ar^{6+} for the $3s^2\ ^1S^e \rightarrow 3s3p\ ^1P^o$ transition at 27.5, 42.2, and 100 eV.

Recently there has been extensive interest in studying the electron-impact excitation of atoms and ions using the electron-photon coincidence technique. In this technique, the polarization of the radiation emitted by the atoms and ions after the electron-impact excitation is detected in coincidence with the scattered electrons. This yields detailed information about the dynamics of the electron-excitation process. In the case of electron-impact excitation to a *P* state, the light emitted on decay of the excited *P* state in one direction is fully described by three Stokes parameters, the two linear polarizations P_1 and P_2, and the circular polarization P_3 [11]. In noncoincidence experiments, where the radiation emitted after deexcitation of the excited *P* states is measured without detecting the scattered electrons, the cross sections of the magnetic substate excitations and the polarization fraction [12] can also be obtained. Such a technique provides detailed information that cannot be obtained from the TCS derived by averaging over the initial magnetic substates and summing over the final magnetic substates. Such magnetic substate excitation data are needed in plasma applications [13].

In a recent paper [14], Kai *et al.* presented a study of electron-impact excitation of the $3s3p\ ^1P^o$ state in Si^{2+}, and reported the TCS, DCS, and Stokes parameters P_1, P_2, and P_3 using the *R*-matrix method with 28 target states. Those TCS calculations were in very good agreement with the available experimental data in the low-energy region. The Stokes parameter P_3 at small angles was also found to have positive values at low energies, while the P_3 for the neutral atom has negative values for similar excitation of a *P* state. The aim of the present paper is to extend the *R*-matrix calculation to other Mg-like ions, in this case S^{4+}, Ar^{6+}, and Ca^{8+}, in order to obtain theoretical TCS, DCS, polarization fraction, and Stokes parameters for the $3s3p\ ^1P^o$ excitation at low incident energies, and to compare them with the available experimental TCS and DCS data. The atomic number (Z) dependence in these results is also investigated, and the feature of positive P_3 at small scattering angles as seen for Si^{2+} is confirmed for other Mg-like ions. Although no experimental data are available for the polarization fraction and Stokes parameters of electron-impact excitation for these Mg-like ions, the present calculations are expected to be valuable in guiding future experiments.

II. THEORETICAL CALCULATIONS

A. Wave functions

Configuration-interaction expansions were used to represent the S^{4+}, Ar^{6+}, and Ca^{8+} target ions, considering the configuration-interaction expansions involving the 77 *LS* terms as listed in Table I. The $1s$, $2s$, $2p$, and $3s$ orbitals used in this work are the Hartree-Fock wave functions given by Clementi and Roetti [15] for the ground state

*Electronic address: shinobu@miyazaki-u.ac.jp

TABLE I. Configurations for each target symmetry used in the present *R*-matrix calculations.

Symmetry	Configuration
$^1S^e$	$3s^2, 3p^2, 3d^2, 3s4s, 3p4p, 3d\overline{4d}, 4s^2, 4p^2, \overline{4d}^2, \overline{4f}^2, 3s\overline{5s}, 4s\overline{5s}$
$^3S^e$	$3s4s, 3p4p, 3d\overline{4d}, 3s\overline{5s}, 4s\overline{5s}$
$^{1,3}P^o$	$3s3p, 3p3d, 3s4p, 3p4s, 3p\overline{4d}, 3d4p, 3d\overline{4f}, 3p\overline{5s}, 4s4p, 4p\overline{4d}, \overline{4d}\,\overline{4f}, 4p\overline{5s}$
$^1D^e$	$3s3d, 3p^2, 3d^2, 3s\overline{4d}, 3p4p, 3p\overline{4f}, 3d4s, 3d\overline{4d}, 3d\overline{5d}, 4s\overline{4d}, 4p^2, 4p\overline{4f}, \overline{4d}^2, \overline{4f}^2$
$^3D^e$	$3s3d, 3s\overline{4d}, 3p4p, 3p\overline{4f}, 3d4s, 3d\overline{4d}, 3d\overline{5s}, 4s\overline{4d}, 4p\overline{4f}$
$^{1,3}F^o$	$3p3d, 3s\overline{4f}$
$^3P^e$	$3p^2, 3d^2, 3p4p, 3d\overline{4d}, 4p^2, \overline{4d}^2, \overline{4f}^2$
$^{1,3}D^o$	$3p3d$

$1s^22s^22p^63s^2\ ^1S^e$. The $3p$, $3d$, $4s$, and $4p$ orbitals are optimized on the energies of the $3s3p\ ^1P^o$, $3s3d\ ^1D^e$, $3s4s\ ^1S^e$, and $3s4p\ ^1P^o$ states, respectively, using the CIV3 atomic structure program of Hibbert [16]. The $\overline{4d}$, $\overline{4f}$, and $\overline{5s}$ pseudo-orbitals are also determined by optimizing on the energies of the $(3s^2+3p^2+3s4s)\ ^1S^e$, $3s3d\ ^1D^e$, and $(3s3p+3p3d+3s4p)\ ^1P^o$ states, respectively, using $\overline{4d}^2\ ^1S^e$, $\overline{4f}^2\ ^1D^e$, and $(3p\overline{5s}+4p\overline{5s})\ ^1P^o$ states.

Table II compares the present excitation energies of S^{4+}, Ar^{6+}, and Ca^{8+} for the $3s3p\ ^1P^o$ states with other theoretical results [9,10,17] and experimental data from the National Institute of Standards and Technology (NIST) website [18]. The present results are in agreement with the experimental data and other theoretical results. The length and velocity forms of the oscillator strength are presented in Table III. Again, the agreement between the present values and other theoretical and experimental results is good.

B. *R*-matrix calculation

Three *R*-matrix calculations were carried out: RM12, RM24, and RM31. Here the number after the letters "RM" indicates the number of coupled target states in the calculation, as listed in Table IV for S^{4+}, Ar^{6+}, and Ca^{8+}. The calculations are performed using the computer program of Berrington *et al.* [19]. The total wave function of the electron + the target ion (with N electrons) system in a sphere with the radius r_a is expanded as

$$\Psi_k = \mathcal{A}\sum_{ij} c_{ijk}\overline{\Phi}_i u_{ij} + \sum_j d_{jk}\chi_j, \tag{1}$$

where $\mathcal{A}$ is the antisymmetrization operator, $\overline{\Phi}_i$ are channel functions representing the target state coupled with the angular and spin functions of the incident electron, χ_j are the $(N+1)$-electron functions constructed from the bound orbitals used for the N-electron target states, and u_{ij} are the continuum orbitals describing the motion of the scattered electron. The coefficients c_{ijk} and d_{jk} in Eq. (1) are obtained by diagonalizing the total Hamiltonian of the whole system within the finite space of the inner region. In the RM31 calculation, the R matrix is calculated on the boundary of a sphere of radius (r_a) 10.6, 8.4, and 7.6 a.u. for S^{4+}, Ar^{6+}, and Ca^{8+}, respectively. A total of 20 continuum orbitals are included for each angular symmetry in order to achieve good convergence in the incident energy range considered. The calculation is carried out for all the partial waves with total angular momentum $L=0$ up to 16. For $r>r_a$, the set of coupled differential equations is solved using the asymptotic code STGF of Berrington *et al.* [20] for the scattering wave functions, which, after matching to the R matrix on the boundary, yields the transition (T) matrix. Partial-wave con-

TABLE II. Excitation energies (in eV) for the $3s3p\ ^1P^o$ state.

	Theory		
Target	Present	Other	Experiment [18]
S^{4+}	15.85	15.91[a]	15.76
Ar^{6+}	21.21	21.20[b]	21.17
Ca^{8+}	26.46	27.07[c]	26.59

[a]Dufton and Kingston [9].
[b]Griffin *et al.* [10].
[c]Tayal [17].

TABLE III. Oscillator strengths for the $3s^2\ ^1S^e \rightarrow 3s3p\ ^1P^o$ transition for S^{4+}, Ar^{6+}, and Ca^{8+}.

	Theory				
	Present result		Other		
Target	Length	Velocity	Length	Velocity	Experiment
S^{4+}	1.449	1.428	1.440[a]		1.46 ± 0.15[b]
					1.46 ± 0.08[c]
					1.46[d]
Ar^{6+}	1.240	1.218	1.236[e]	1.226[e]	
Ca^{8+}	1.083	1.060	1.078[e]	1.065[e]	

[a]Almaraz *et al.* [32].
[b]Wiese *et al.* [29].
[c]Reistad *et al.* [30].
[d]Joelsson *et al.* [31].
[e]Tayal [17].

TABLE IV. Target states used in the various R-matrix calculations for S^{4+} and Ar^{6+}. For Ca^{8+}, $3d^2$ was included instead of $3p4p$, and $3d4s$ instead of $3s4d$.

Symmetry	RM12	RM24	RM31
$^1S^e$	$3s^2, 3p^2, 3s4s$	$3s^2, 3p^2, 3s4s$	$3s^2, 3p^2, 3s4s, 3p4p, 3s\overline{5s}$
$^3S^e$	$3s4s$	$3s4s$	$3s4s, 3p4p, 3s\overline{5s}$
$^1P^o$	$3s3p, 3s4p$	$3s3p, 3s4p, 3p4s, 3p3d$	$3s3p, 3s4p, 3p4s, 3p3d$
$^3P^o$	$3s3p, 3s4p$	$3s3p, 3s4p, 3p4s, 3p3d$	$3s3p, 3s4p, 3p4s, 3p3d$
$^1D^e$	$3p^2, 3s3d$	$3p^2, 3s3d, 3s\overline{4d}$	$3p^2, 3s3d, 3s\overline{4d}, 3p4p$
$^3D^e$	$3s3d$	$3s3d, 3s\overline{4d}$	$3s3d, 3s\overline{4d}, 3p4p$
$^{1,3}F^o$		$3p3d, 3s\overline{4f}$	$3p3d, 3s\overline{4f}$
$^3P^e$	$3p^2$	$3p^2$	$3p^2, 3p4p$
$^{1,3}D^o$		$3p3d$	$3p3d$

tributions for $L>17$ in the calculation of the TCS are estimated by a top-up procedure using a geometric series, while for the contributions in the calculations of the DCS, the polarization fraction and Stokes parameters are estimated if necessary by extrapolating the T matrices to obtain those for $L>17$.

Using the T matrix, the scattering amplitude with the Fano and Racah phase convention for excitation from an initial state N_i to a final state N_f in an electron-ion collision is given by

$$\begin{aligned} f(N_i{:}L_iM_i\Pi_iM_{s_i}m_{s_i}M \rightarrow N_f{:}L_fM_f\Pi_fM_{s_f}m_{s_f}M) \\ = i\sum_{l_il_fLS\Pi}\frac{\pi^{1/2}}{(k_ik_f)^{1/2}}(2l_i+1)^{1/2}e^{i(\sigma_{l_i}+\sigma_{l_f})} \\ \times\langle L_il_iM_i0|LM\rangle\langle LM|L_fl_fM_fm_f\rangle \\ \times\left\langle S_i\tfrac{1}{2}M_{s_i}m_{s_i}|SM_s\right\rangle\left\langle SM_s|S_f\tfrac{1}{2}M_{s_f}m_{s_f}\right\rangle \\ \times T^{LS\Pi}_{l_il_f}(N_i\rightarrow N_f)Y_{l_fm_f}(\theta), \end{aligned} \tag{2}$$

where

$$\sigma_{l_i} = \arg\Gamma(l_i+1+i\eta_i), \quad \eta_i = z/k_i,$$

$$\sigma_{l_f} = \arg\Gamma(l_f+1+i\eta_f), \quad \eta_f = z/k_f,$$

$$z = -(Z-N). \tag{3}$$

Here, L is the total angular momentum, M is the z component of total angular momentum, Π is the total parity, l_i is the incident electron angular momentum, l_f is the scattering electron angular momentum, m_f is the z component of the scattering electron angular momentum, m_{s_i} is the z component of the incident electron spin momentum, m_{s_f} is the z component of the scattered electron spin momentum, k_i is the incident electron wave number, and k_f is the scattered electron wave number. The N_i and N_f states of the target are characterized by their orbital angular momenta L_i and L_f with components M_i and M_f along the z axis, spin momenta S_i and S_f with z-axis components M_{s_i} and M_{s_f}, and parities Π_i and Π_f.

C. Cross sections

The DCS for the $3s^2\ ^1S^e \rightarrow 3s3p\ ^1P^o$ transition at a fixed scattering angle θ is given by

$$\sigma = \sigma_0 + 2\sigma_1, \tag{4}$$

where

$$\sigma_{M_f} = \frac{k_f}{2k_i(2L_i+1)(2S_i+1)}\sum_{M_iM_{s_i}M_{s_f}m_fm_{s_i}m_{s_f}}|f(N_i\rightarrow N_f)|^2. \tag{5}$$

Here, σ_{M_f} $(M_f=0,1)$ is the DCS for the excitation of magnetic sublevel M_f of the $3s3p\ ^1P^o$ state.

The TCS is given by

$$Q = Q_0 + 2Q_1, \tag{6}$$

where

$$Q_{M_f} = 2\pi\int_0^\pi \sigma_{M_f}\sin\theta\, d\theta. \tag{7}$$

Here, Q_{M_f} $(M_f=0,1)$ is the TCS for the excitation of magnetic sublevel M_f of the $3s3p\ ^1P^o$ state.

D. Polarization fraction and Stokes parameters

The incident electrons are assumed to travel in the positive z direction to be scattered through an angle θ in the xz plane. The polarization fraction for radiation emitted in the y direction without detecting the scattered electron is then defined by

$$P = \frac{I_\parallel - I_\perp}{I_\parallel + I_\perp}, \tag{8}$$

where $I_\parallel$ $(I_\perp)$ is the intensity of photons with electric vectors parallel (perpendicular) to the beam direction. For radiation from the $3s3p\ ^1P^o \rightarrow 3s^2\ ^1S^e$ line of Mg-like ions, we have [12]

$$P = \frac{Q_0 - Q_1}{Q_0 + Q_1}. \tag{9}$$

The Stokes parameters P_i $(i=1-3)$ depend on the scattering angles θ. These scattered electrons are detected in coincidence with photons emitted in the y direction by the subsequent decay [11]. The linear polarizations P_1 and P_2 and circular polarization P_3 are defined by

$$P_1 = \frac{I(0\,^\circ) - I(90\,^\circ)}{I(0\,^\circ) + I(90\,^\circ)}, \tag{10}$$

$$P_2 = \frac{I(45\,^\circ) - I(135\,^\circ)}{I(45\,^\circ) + I(135\,^\circ)}, \tag{11}$$

and

$$P_3 = \frac{I(\mathrm{RHC}) - I(\mathrm{LHC})}{I(\mathrm{RHC}) + I(\mathrm{LHC})}, \tag{12}$$

where $I(\alpha)$ is the intensity of light with the polarization detector in the α direction with respect to the incident electron direction, and I(RHC) and I(LHC) are the intensities of the right-handed and left-handed circularly polarized light components.

The Stokes parameters P_i $(i=1-3)$ can be expressed as given below in terms of state multipoles of the electron-impact excited state (i.e., P states of the ions) which are related to the scattering amplitude or the T matrix. In general, for photon decay in the transition $L_f \rightarrow L_j$, we can write the following [21]:

$$P_1 = \frac{1}{I}\begin{Bmatrix} 1 & 1 & 2 \\ L_f & L_f & L_j \end{Bmatrix}\left(\sqrt{\frac{3}{2}} G_2(L_f)\langle T(L_f)^+_{20}\rangle - G_2(L_f)\langle T(L_f)^+_{22}\rangle \right), \tag{13}$$

$$P_2 = -\frac{2}{I}\begin{Bmatrix} 1 & 1 & 2 \\ L_f & L_f & L_j \end{Bmatrix} G_2(L_f)\langle T(L_f)^+_{21}\rangle, \tag{14}$$

and

$$P_3 = \frac{2i}{I}\begin{Bmatrix} 1 & 1 & 1 \\ L_f & L_f & L_j \end{Bmatrix} G_1(L_f)\langle T(L_f)^+_{11}\rangle, \tag{15}$$

where

$$I = \frac{2(-1)^{L_j+L_f}}{3\sqrt{2L_f+1}} G_0(L_f)\langle T(L_f)^+_{00}\rangle + \begin{Bmatrix} 1 & 1 & 2 \\ L_f & L_f & L_j \end{Bmatrix} \times \left(\frac{G_2(L_f)}{\sqrt{6}}\langle T(L_f)^+_{20}\rangle + G_2(L_f)\langle T(L_f)^+_{22}\rangle \right). \tag{16}$$

The fine-structure depolarization coefficient $G_K(L_f)$ can be written as

$$G_K(L_f) = \frac{1}{(2S_f+1)}\sum_J (2J+1)^2 \begin{Bmatrix} L_f & J & S \\ J & L_f & K \end{Bmatrix}. \tag{17}$$

Here, $J=L_f+S_f$ is the total angular momentum quantum number of the atom. The $G_K(L_f)$ is normalized such that $G_0(L_f)=1$ for all L_f. Since we are considering excitation to the ^1P states only, all the $G_K(L_f)$ values are unity. The value of L_j corresponds to the total angular momentum quantum number of the state to which the excited atoms in the $^1P^o$ state decay. The state multipoles are defined by

$$\langle T(L_f)^+_{KQ}\rangle = \sum_{M'_f M_f} (-1)^{L_f - M_f}\langle LLM'_f - M_f | KQ\rangle \langle f_{M'_f} f_{M_f}\rangle, \tag{18}$$

$$\langle f_{M'_f} f_{M_f}\rangle = \frac{k_f}{2k_i(2S_i+1)} \sum_{m_{s_i} m_{s_f} M_{s_i} M_{s_f}} f(N_i \rightarrow N'_f) f(N_i \rightarrow N_f)^*, \tag{19}$$

where $0 \leqslant K \leqslant 2L_f$ and $-K \leqslant Q \leqslant K$. Here, $\langle T(L_f)^+_{00}\rangle$ is a measure of the overall population of the atomic state, and $\langle T(L_f)^+_{1Q}\rangle$ and $\langle T(L_f)^+_{2Q}\rangle$ describe the orientation and alignment of the excited target ion.

III. RESULTS AND DISCUSSION

A. Cross sections

In the calculation of the TCS for the $3s^2\,{}^1S^e \rightarrow 3s3p\,{}^1P^o$ transition in S^{4+}, Ar^{6+}, and Ca^{8+} using the R-matrix method,

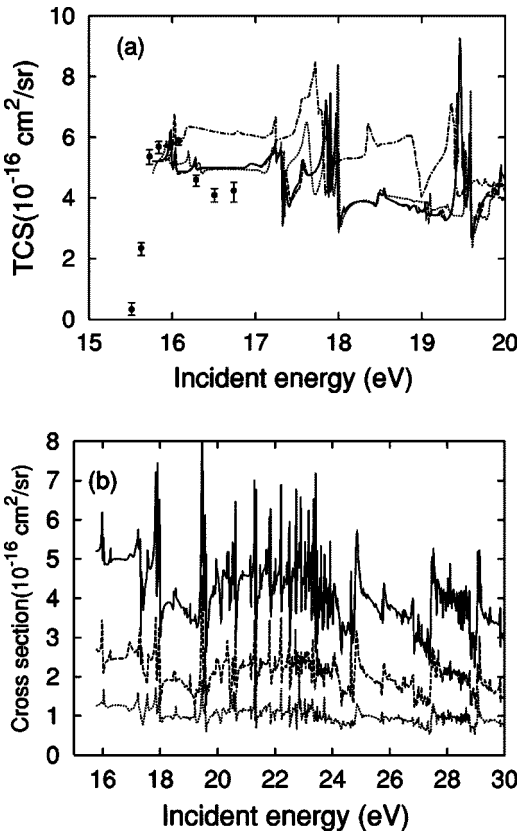

FIG. 1. (a) Total cross sections for the $3s^2\,{}^1S^e \rightarrow 3s3p\,{}^1P^o$ transition from threshold to 20 eV in S^{4+}. Theory:—, RM31 results; - - -, RM24 results; …… , RM12 results;- . -, Dufton and Kingston [9]. Experiment: ●, Wallbank *et al.* [8]. (b) Cross sections of RM31 results for the $3s^2\,{}^1S^e \rightarrow 3s3p\,{}^1P^o$ transition from threshold to 30 eV in S^{4+}:—, Q; - - -, Q_0; …… , Q_1.

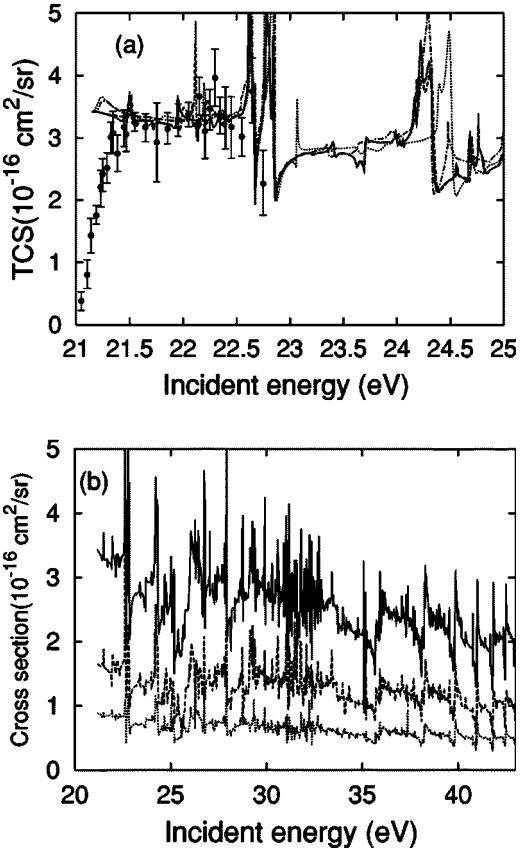

FIG. 2. (a) Total cross sections for the $3s^2\ ^1S^e \rightarrow 3s3p\ ^1P^o$ transition from threshold to 25 eV in Ar^{6+}. Theory:—, RM31 results; - - -, RM24 results; …… , RM12 results; - . -, Griffin *et al.* [10]. Experiment: ●, Chung *et al.* [3]. (b) Cross sections of RM31 results for the $3s^2\ ^1S^e \rightarrow 3s3p\ ^1P^o$ transition from threshold to 42 eV in Ar^{6+}:—, Q; - - -, Q_0; …… , Q_1.

the excited state energies were adjusted using observed energies [18] to allow the present results to be compared with experimental results. Figure 1(a) shows the TCS results for the $3s^2\ ^1S^e \rightarrow 3s3p\ ^1P^o$ transition in S^{4+} in the RM12, RM24, and RM31 calculations. The eight-state R-matrix calculation of Dufton and Kingston [9] and the experimental results of Wallbank *et al.* [8] are also shown in the figure. The differ-

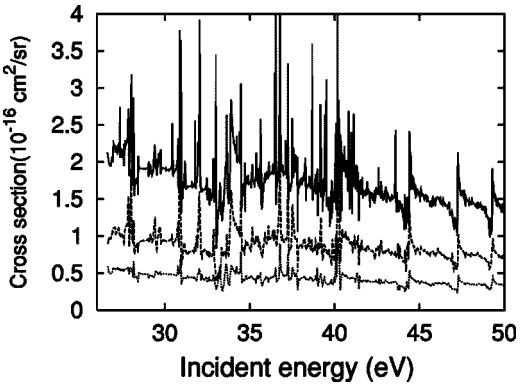

FIG. 3. Cross sections of RM31 results for the $3s^2\ ^1S^e \rightarrow 3s3p\ ^1P^o$ transition from threshold to 50 eV in Ca^{8+}:—, Q; - - -, Q_0; …… , Q_1.

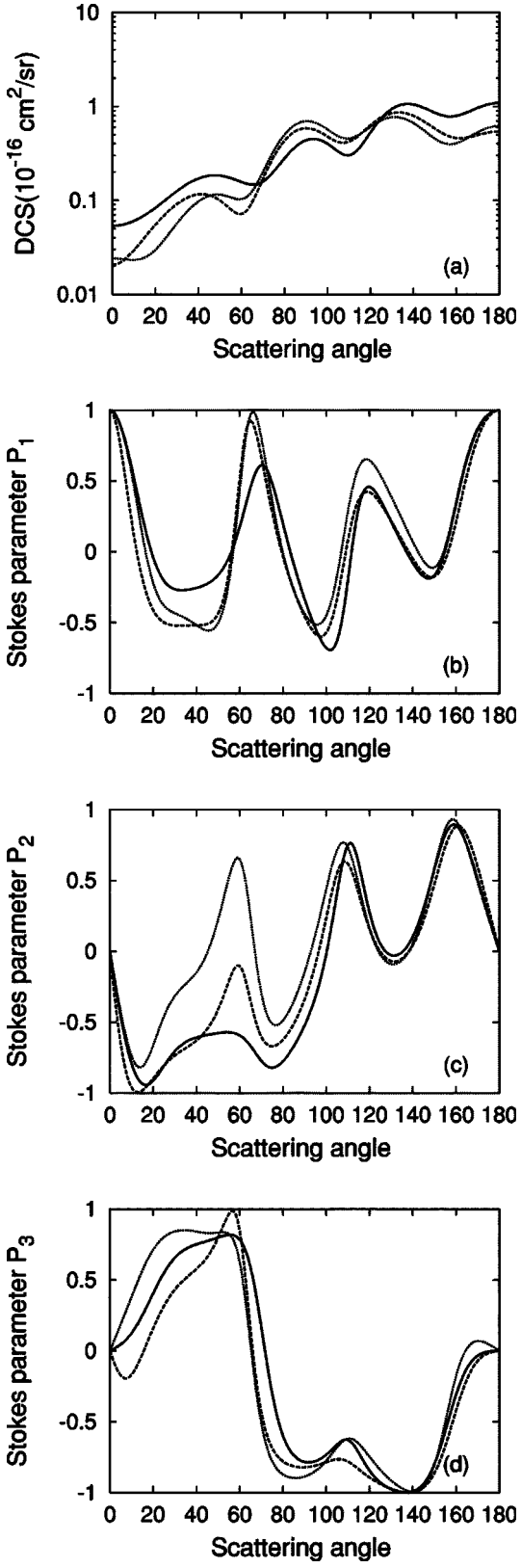

FIG. 4. Differential cross sections and Stokes parameters for the $3s^2\ ^1S^e \rightarrow 3s3p\ ^1P^o$ transition in S^{4+}. (a) Differential cross sections:—, 15.8 eV; - - -, 16.4 eV; …… , 17.0 eV. (b) Same as for (a) but Stokes parameter P_1. (c) Same as for (a) but Stokes parameter P_2. (d) Same as for (a) but Stokes parameter P_3.

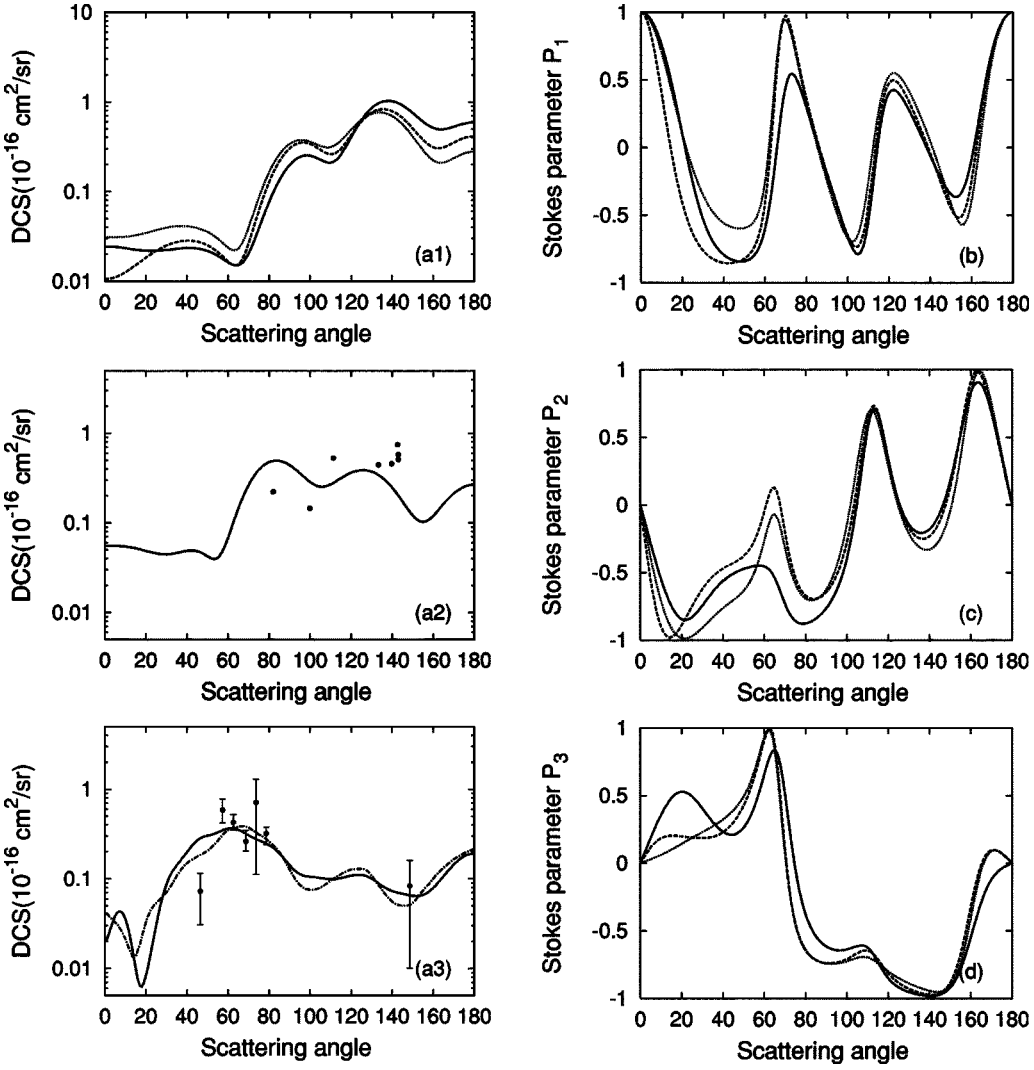

FIG. 5. Differential cross sections and Stokes parameters for the $3s^2\ ^1S^e \rightarrow 3s3p\ ^1P^o$ transition in Ar^{6+}. (a1) Differential cross sections:—, 21.2 eV; - - -, 21.6 eV; …… , 22.0 eV. (a2) Differential cross sections at 27.5 eV. Theory:—, RM31 results. Experiment: ●, Jalabert *et al.* [2]. (a3) Differential cross sections at 42.2 eV. Theory:—, RM31 results; - . -, Griffin *et al.* [10]. Experiment: ●, Jalabert *et al.* [2]. (b) Same as for (a) but Stokes parameter P_1. (c) Same as for (a) but Stokes parameter P_2. (d) Same as for (a) but Stokes parameter P_3.

ence between RM24 and RM31 calculations is in general smaller than the difference between RM12 and RM24 calculations, indicating an apparent convergence with respect to the number of target states included in the calculations. Consequently, the RM31 calculation is considered the most reliable. On comparing the results in the figure, the *R*-matrix results of Dufton and Kingston [9] are generally larger than the present results. The agreement between the present results and the experimental results of Wallbank *et al.* [8], where the resonance contributes significantly to the cross section near threshold, is extremely good in the energy region up to about 16.3 eV. However, the present results are slightly higher at 16.5 and 16.7 eV. Figure 1(b) shows the present TCS, Q_0, and Q_1 results for S^{4+} in the RM31 calculation from threshold to 30 eV.

Figure 2(a) presents the TCS for the $3s^2\ ^1S^e \rightarrow 3s3p\ ^1P^o$ transition in Ar^{6+} in the RM12, RM24, and RM31 calculations for comparison with the eight-state *R*-matrix calculation of Griffin *et al.* [10] and the experimental results of Chung *et al.* [3]. All the theoretical results are reasonably consistent with the available experimental data at all energies represented by the experimental data. Figure 2(b) shows the TCS, Q_0, and Q_1 results for the target of Ar^{6+} from threshold to 42 eV.

As no theoretical or experimental data are available for the $3s^2\ ^1S^e \rightarrow 3s3p\ ^1P^o$ transition in Ca^{8+}, only the RM31 results for Ca^{8+} (TCS, Q_0, and Q_1) are shown in Fig. 3 for the energy range from threshold to 50 eV. All the results for Ca^{8+} exhibit similar behavior to that of S^{4+} and Ar^{6+}.

B. Differential cross section and Stokes parameters

In the previous report [14] for Si^{2+}, the nature of the variation in the Stokes parameters P_i $(i=1-3)$ was found to

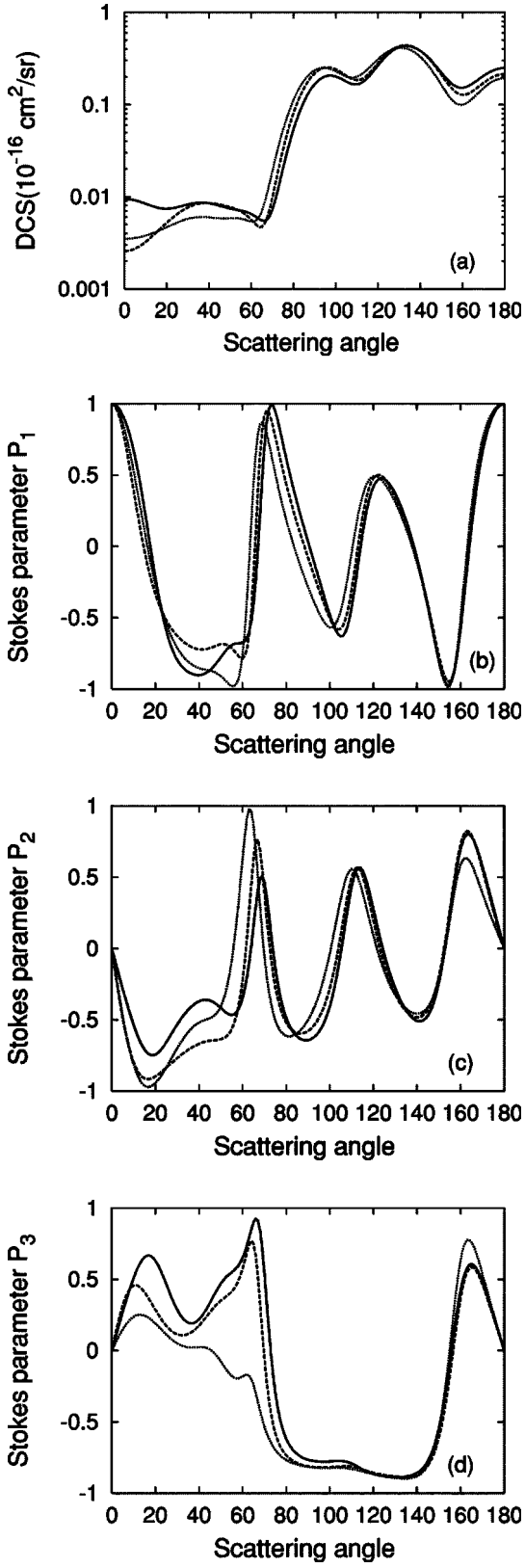

FIG. 6. Differential cross sections and Stokes parameters for the $3s^2\ ^1S^e \rightarrow 3s3p\ ^1P^o$ transition in Ca^{8+}. (a) Differential cross sections:—, 28.3 eV; ---, 28.7 eV; ……, 30.0 eV. (b) Same as for (a) but Stokes parameter P_1. (c) Same as for (a) but Stokes parameter P_2. (d) Same as for (a) but Stokes parameter P_3.

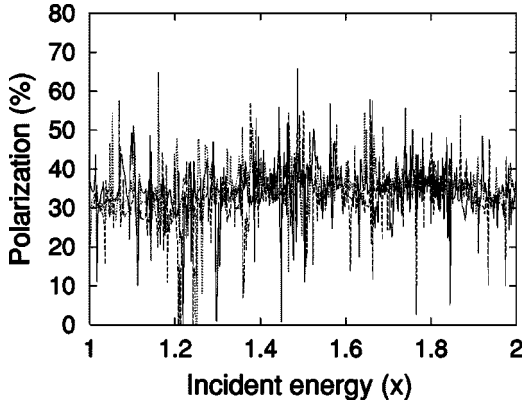

FIG. 7. Polarization fractions of the $3s3p\ ^1P^o \rightarrow 3s^2\ ^1S^e$ line of the Mg-like ions, as a function of X (the incident energy in threshold units):—, S^{4+}; ---, Ar^{6+}; ……, Ca^{8+}.

change dramatically with energy in the resonance region, yet to remain very stable in the nonresonance region. The DCS and Stokes parameters for S^{4+}, Ar^{6+}, and Ca^{8+} in the RM31 calculation are shown here for the nonresonance region at low incidence energy. Figure 4(a) shows the DCS as a function of scattering angle for the $3s^2\ ^1S^e \rightarrow 3s3p\ ^1P^o$ transition in S^{4+} at incident energies of 15.8, 16.4, and 17.0 eV. The DCS of Ar^{6+} is shown in Fig. 5(a1) at 21.2, 21.6, and 22.0 eV. The present results at 27.5 and 42.2 eV are compared with the experimental results of Jalabert *et al.* [2] in Figs. 5(a2) and (a3). The simple two-state calculations of Griffin *et al.* [10] are also compared in Fig. 5(a3). As can be seen in both figures, the present results are in good agreement with the experiments.

Figure 6(a) shows the DCS of Ca^{8+} at 28.3, 28.7, and 30.0 eV. Although the values of the DCS for S^{4+} increase slowly at 15.8, 16.4, and 17.0 eV with increasing scattering angle, the values of the DCS for Ca^{8+} increase rapidly (near 70°) at 28.3, 28.7, and 30 eV. For S^{4+}, Ar^{6+}, and Ca^{8+}, backward scattering is dominant in the $3s^2\ ^1S^e \rightarrow 3s3p\ ^1P^o$ transition at low incidence energies, proportional to the increasing ionic charge. This was also reported by Nakazaki *et al.* [22] for the $3s\ ^2S^e \rightarrow 3p\ ^2P^o$ transition in Na-like ions.

Figures 4(b)–4(d), 5(b)–5(d), and 6(b)–6(d) show the Stokes parameters (P_1, P_2, and P_3) as a function of scattering angle for S^{4+}, Ar^{6+}, and Ca^{8+}. The results for the Stokes parameter P_3 in Figs. 4(d), 5(d), and 6(d) are the same as those for Si^{2+}, as shown in the previous report [14]. P_3, which represents the circular polarization, is equivalent to $-L_\perp$, the angular momentum transfer to the excited state of the target. According to the propensity rule of $L_\perp$, $L_\perp$ is positive at small scattering angles (i.e., P_3 is negative) in electron-atom collisions. Thus, it should be noted that the Stokes parameter P_3 at small angles is positive in the Mg-like ions.

C. Polarization fraction

The emission line from the $^1P^o \rightarrow {}^1S^e$ transition in neutral atoms is predicted to be 100% linearly polarized at threshold [12]. Polarization fractions have been studied both experi-

mentally and theoretically for electron–He-like-ion collisions [23–28]. The low-charge He-like ions are polarized about 60% near threshold. Figure 7 shows the polarization fractions as a function of incident-electron energy for the $3s3p\ ^1P^o \rightarrow 3s^2\ ^1S^e$ line of the Mg-like ions S^{4+}, Ar^{6+} and Ca^{8+}. The resulting polarization fraction for Mg-like ions is polarized about 35% at $X=1-2$, where X is the incidence energy in threshold units. The polarization fraction is almost independent of nuclear charge. However, the behavior of the polarization fractions of the $3s3p\ ^1P^o \rightarrow 3s^2\ ^1S^e$ line in the Mg-like ions is very different from that of the $1s2p\ ^1P^o \rightarrow 1s^2\ ^1S^e$ line in He-like ions.

IV. CONCLUSIONS

The total cross sections, differential cross sections, Stokes parameters, and polarization fractions were calculated using the R-matrix method with 31 target states (RM31) for the $3s^2\ ^1S^e \rightarrow 3s3p\ ^1P^o$ transition of S^{4+}, Ar^{6+}, and Ca^{8+} in the low-energy region. The present results are in very good agreement with the experiment results of Wallbank *et al.* [8] for the TCS near threshold. Backward scattering was found to be dominant for the DCS at low incidence energy, proportional to increasing ionic charge. The Stokes parameter P_3 at small angles has positive values at low energies for the excitation in S^{4+}, Ar^{6+}, and Ca^{8+}. The resulting polarization fraction for Mg-like ions gives polarization of about 35% at $X=1-2$.

ACKNOWLEDGMENTS

This research was partially supported by the Ministry of Education, Culture, Sports, Science and Technology, Japan, through a Grant-in-Aid for Scientific Research (C) (S.N.).

[1] I. D. Williams, Rep. Prog. Phys. **62**, 1431 (1999).
[2] D. Jalabert, C. Ristori, M. Maurel, J. C. Rocco, and B. A. Huber, Nucl. Instrum. Methods Phys. Res. B **98**, 132 (1995).
[3] Y.-S. Chung, N. Djurić, B. Wallbank, G. H. Dunn, M. E. Bannister, and A. C. H. Smith, Phys. Rev. A **55**, 2044 (1997).
[4] B. Wallbank, N. Djurić, O. Woitke, S. Zhou, G. H. Dunn, A. C. H. Smith and M. E. Bannister, Phys. Rev. A **56**, 3714 (1997).
[5] D. B. Reisenfeld, L. D. Gardner, P. H. Janzen, D. W. Savin, and J. L. Kohl, Phys. Rev. A **60**, 1153 (1999).
[6] N. Djurić, M. E. Bannister, A. M. Derkatch, D. C. Griffin, H. F. Krause, D. B. Popović, A. C. H. Smith, B. Wallbank, and G. H. Dunn, Phys. Rev. A **65**, 052711 (2002).
[7] P. H. Janzen, L. D. Gardner, D. B. Reisenfeld, and J. L. Kohl, Phys. Rev. A **67**, 052702 (2003).
[8] B. Wallbank, M. E. Bannister, Y.-S. Chung, N. Djurić, G. H. Dunn, H. F. Krause, and A. C. H. Smith, in *Abstracts of Contributed Papers, XXIII International Conference on Photonic, Electronic and Atomic Collisions*, edited by Josef Anton, Henrik Cederquist, Mats Larsson, Eva Lindroth, Sven Mannervik, Henning Schmidt, and Reinhold Schuch (Stockholm University, Stockholm, 2003).
[9] P. L. Dufton and A. E. Kingston, J. Phys. B **17**, 3321 (1984).
[10] D. C. Griffin, M. S. Pindzola, and N. R. Badnell, Phys. Rev. A **47**, 2871 (1993).
[11] N. Andersen, J. W. Gallagher, and I. V. Hertel, Phys. Rep. **279**, 251 (1988).
[12] I. C. Percival and M. J. Seaton, Philos. Trans. R. Soc. London, Ser. A **251**, 113 (1958).
[13] T. Fujimoto and S. A. Kazantsev, Plasma Phys. Controlled Fusion **39**, 1267 (1997).
[14] T. Kai, R. Srivastava, and S. Nakazaki, J. Phys. B **37**, 2045 (2004).
[15] E. Clementi and C. Roetti, At. Data Nucl. Data Tables **14**, 177 (1974).
[16] A. Hibbert, Comput. Phys. Commun. **9**, 141 (1975).
[17] S. S. Tayal, J. Phys. B **19**, 3421 (1986).
[18] See http://physics.nist.gov/cgi-bin/AtData/levels_form
[19] K. A. Berrington, W. B. Eissner, and P. H. Norrington, Comput. Phys. Commun. **92**, 290 (1995).
[20] K. A. Berrington, P. G. Burke, K. Butler, M. J. Seaton, P. J. Storey, K. T. Taylor, and Y. Yan, J. Phys. B **20**, 6379 (1987).
[21] K. Blum, *Density Matrix Theory and Applications*, 2nd ed. (Plenum, New York, 1996).
[22] S. Nakazaki, S. Yonezawa, E. Kimura, and Y. Itikawa, Phys. Scr., T **73**, 127 (1997).
[23] J. R. Henderson, P. Beiersdorfor, C. L. Bennett, S. Chantrenne, D. A. Knapp, R. E. Marrs, M. B. Schneider, K. L. Wong, G. A. Doschek, J. F. Seely, C. M. Brown, R. E. LaVilla, J. Dubau, and M. A. Levine, Phys. Rev. Lett. **65**, 705 (1990).
[24] P. Beiersdorfer, D. A. Vogel, K. J. Reed, V. Decaux, J. H. Scofield, K. Widmann, G. Hölzer, E. Förster, O. Wehrhan, D. W. Savin, and L. Schweikhard, Phys. Rev. A **53**, 3974 (1996).
[25] P. Beiersdorfer, G. Brown, S. Utter, P. Neill, K. J. Reed, A. J. Smith, and R. S. Thoe, Phys. Rev. A **60**, 4156 (1999).
[26] M. K. Inal and J. Dubau, J. Phys. B **20**, 4221 (1987).
[27] Y. Itikawa, R. Srivastava, and K. Sakimoto, Phys. Rev. A **44**, 7195 (1991).
[28] K. J. Reed and M. H. Chen, Phys. Rev. A **48**, 3644 (1993).
[29] W. L. Wiese, M. W. Smith, and B. M. Miles, *Atomic Transition Probabilities*, Natl. Bur. Stand. Ser Ref. Data Series, Natl. Bur. Stand. Circ. No. 22 (U.S. GPO, Washington, DC, 1969), Vol. 2.
[30] N. Reistad, T. Brage, J. O. Ekberg, and L. Engström, Phys. Scr. **30**, 249 (1984).
[31] I. Joelson, P. O. Zetterberg, and C. E. Magnusson, Phys. Scr. **23**, 1087 (1981).
[32] M. A. Almaraz, A. Hibbert, C. Lavin, I. Martin, and K. L. Bell, J. Phys. B **33**, 3277 (2000).